Shock adhesion test for composite bonded assembly using a high pulsed power generator

Elise Gay, Laurent Berthe, Eric Buzaud, M Boustie, M. Arrigoni

HAL Id: hal-00987470
https://hal.archives-ouvertes.fr/hal-00987470

Shock adhesion test for composite bonded assembly using a high pulsed power generator

E. Gay,[1,a)] L. Berthe,[1] E. Buzaud,[2] M. Boustie,[3] and M. Arrigoni[4]

[1]*Laboratoire Procédés et Ingénierie en Mécanique et Matériaux (CNRS), Arts et Métiers ParisTech,*
151 bd de l'Hôpital, 75013 Paris, France
[2]*CEA Gramat, 46500 Gramat, France*
[3]*Département Physique et Mécanique des Matériaux, Institut Pprime (CNRS) ENSMA, 1 av. Clément Ader,*
86960 Futuroscope Cedex, France
[4]*Laboratoire Brestois de Mécanique et des Systèmes EA 4325, ENSTA Bretagne, 2 rue François Verny,*
29806 Brest Cedex 9, France

In a context of the rising use of composite assemblies in aeronautic or defense fields, the assessment of their strength is a key issue. The method developed in this study attempts to provide solutions. A shock adhesion test based on short compressive loads, obtained by a high pulsed power generator, is proposed as a proof test to ensure the quality of composite bonded assemblies. A calibrated load induces a local tensile stress able to damage the bond interface. The high pulsed power source is the GEnerateur de Pression Isentropique device (Isentropic Pressure Generator), used to generate the required stresses, with a 450 ns pulse duration to test assemblies above the mm thickness range. The understanding of the mechanisms of wave propagation and tensile stress generation within these multilayer assemblies are scientific challenges. The ability of the technique to induce a tensile stress able to disbond the laminates and the assemblies is demonstrated. This paper details the response of carbon epoxy laminates and their bonded assemblies to a shock loading near the damage threshold.

I. INTRODUCTION

Lightweight composite materials are widely used as a substitute for metal alloys in many industrial fields, especially for aircraft structures. Adhesive bonding is the preferential way to assemble the laminates to each other. The question of the reliability of bond strength remains because conventional nondestructive inspection techniques are not sensitive to weak or kissing bond (dissociated surfaces in contact) (Pethrick, 2000). Ultrasonic inspection, shear wave, thermography, or coin-tap are able to detect voids or cracks at the interface but cannot easily detect an adhesion leak (Rokhlin and Marom, 1986; Adams and Cawley, 1988; Adams and Drinkwater, 1999). Although ultrasonic spectrometry has provided relevant results in the detection of poor cohesive strength, it is not able to induce a mechanical solicitation to verify the strength at the interfaces (Guyott and Cawley, 1988). Other techniques such as peel-test can ensure that the adhesive joints meet minimal strength but they require the destruction of the specimen. Adhesive bonding is thus not a solution for critical parts of aircraft structures and the bonds have to be secured with mechanical fasteners that contribute to the mass penalty.

An alternative for this industrial challenge is the adhesion test using shock waves, which have the ability to generate tensile stress within a sample and particularly at the interface between two materials (Vossen, 1978). A high pressure pulse drives a compressive wave within the specimen to

test (loading), followed by a release which relaxes the material to its initial state (unloading). This pulse propagates through the material thickness, until reaching the opposite surface. It is reflected back as a tensile wave. In the acoustic approximation for a homogeneous material, the maximal tensile stress begins at a distance of $C_0 \times \tau/2$ from the back surface (Antoun *et al.*, 2003) (C_0 is the bulk sound velocity, τ is the pressure pulse duration). This tensile stress is induced by the reflection of the incident wave crossing the incident release waves. It is possible to monitor and locate this solicitation. It is able to induce damage, called spallation, depending on the load amplitude, the pulse duration and the sample thickness.

The proof-test presented in this study uses this high strain rate solicitation to load locally the interface between two composite plates. This load is normal to the interfaces. A strong interface will remain unaffected, whereas a weak one will fail with the possibility to detect it using velocity suitable diagnostic at the surface opposite to the impact. In fact, each compressive wave reaching the free surface accelerates it, and conversely, the arrival of a tensile wave induces a deceleration.

Such a test is non-destructive when the generated stress does not exceed a prescribed threshold stress. This threshold is estimated by subjecting similar samples to several pulses. The load is increased until the disbond is detected. The damage threshold corresponds to the dynamic tensile strength. It is evaluated using an inverse approach based on numerical simulations of the experiments.

Up to now, many demonstrations of this shock adhesion test have been performed using laser-induced shock. They

---

concern very thin coatings (10–100 μm thick) for which a shock duration in the ns range is adapted (Gupta *et al.*, 1990; Bolis *et al.*, 2007; Arrigoni *et al.*, 2013), or composite laminates (Gilath *et al.*, 1990; Gupta *et al.*, 1996; Yu and Gupta, 1998; Perton *et al.*, 2010; Gay, 2011; Gay *et al.*, 2012). Although this method enables to detect kissing bonds, a pulse duration of a few hundreds of ns is required for thicker structures such as bonded assemblies (Bossi *et al.*, 2004; Bossi *et al.*, 2005). This longer pulse will be less diffused when propagating. Hereby, we propose to use the GEPI facility ("GEnerateur de Pression Isentropique" in French, i.e., Isentropic Pressure Generator, CEA, Gramat) with a 450 ns pulse duration, to induce high amplitude loadings. In our work configuration, the shock loading is destructive since the samples have to be glued to the device. However, this study aims to demonstrate the feasibility of the adhesion test using this brief load. This study could help for the future design of a high power pulsed laser able to produce the same effects, with a nondestructive and industrial mind.

In multilayer materials such as composite laminates or bonded assemblies, the wave propagation is modified by the transmitted and reflected waves at each interface due to the impedance mismatch at each layer (Abrate, 1998; Parga-Landa *et al.*, 1999; Datta, 2000). The impedance is here defined as the product of density and sound velocity of the medium. The material anisotropy also affects the wave propagation and its consecutive damage (De Rességuier *et al.*, 2005; Millett *et al.*, 2007).

This paper deals with the experimental and numerical study of CFRP (Carbon Fibre Reinforced Polymer) assemblies under shock loading produced by the GEPI device. An analysis is conducted to understand the wave propagation within these multi-layer materials using numerical simulations. The goal is the development of an adhesion test of bonded CFRP using intense brief loads.

Section II describes the materials involved in this study and the GEPI facility. The wave propagation is illustrated in Sec. III with an ABAQUS$^{\copyright}$ explicit numerical simulation. As a first step, the tensile stress generation within a CFRP laminate is investigated in Sec. IV. The analysis of the behaviour of composite bonded assemblies under short load is then provided in Sec. V. The sensitivity of the technique to the bond strength is finally discussed in Sec. VI with two different structural adhesives of different strength (FM73 and EA9394).

II. EXPERIMENTAL CONFIGURATION

A. Samples

CFRP specimens are unidirectional plies of carbon fibres (G40-800-24 K) reinforced epoxy (Cytec$^{\circledR}$ 5276-1). They are stacked in oriented layers in the standard configuration $[0/-45/90/45°]_S$. This 8 plies laminate is 1.35 mm thick. The average diameter of the carbon fibres is 5 μm. They represent 70% of the volume. A 30 μm thick interply epoxy layer provides adhesion between plies. This epoxy layer is also observed at the surface of the laminate.

Baseline assemblies are 8 plies laminates bonded together with a total thickness up to 3 mm and cut to 15 ×

15 mm samples. These samples are representative of industrial applications in aeronautic field. Two kinds of bonds have been prepared, respectively, with

- Loctite Hysol$^{\circledR}$ EA9394 (Loctite, 2002). It is a two-component epoxy adhesive with polyimide nodules mixed in the standard hardener-to-resin ratio of 7:100. The thickness of the bond varies from 220 to 260 μm even if wedges have been disposed between the laminates.
- Cytec$^{\circledR}$ FM73 (Cytec FM73, 2009). It is an epoxy/cyanamid adhesive film that requires an additional cure process in an autoclave. The composite laminates of these assemblies have been subjected to a second heat treatment that may modify their mechanical properties. The thickness of the bond is approximately 500 μm.

Quasi-static peel tests have been performed on these samples. The assemblies bonded with FM73 are stronger than the ones made with EA9394: peel strength has been measured at, respectively, 2810 N m^{-1} and 736 N m^{-1}.

B. Load generation

The load is generated by the high pulsed power generator GEPI (Isentropic Pressure Generator, CEA Gramat), providing a 3.5 Mega Ampere current. This generator consists of a RLC circuit that discharges in an aluminum strip-line insulated by a dielectric foil. It is patented by the company ITHPP (ITHPP, 1999; Frescaline and Avrillaud, 2005).

It provides short compressive loading with a 450 ns duration for the first pulse at full width at half maximum, with less important reloads of similar duration. The aluminium electrode that delivers the load is shown in Figure 1(a). The evolution of the incident pressure $P(t)$ is plotted in Figure 1(b) from relation (1) with an error inferior to 10% (Hereil and Avrillaud, 2006).

$$P(t) = k_p \frac{\mu_0}{2} \left(\frac{I(t)}{w} \right)^2, \qquad (1)$$

where k_p is the coefficient for the correction of the pressure diminution due to edge effects in the final strip line, μ_0 is the magnetic permeability, w is the width of the electrode (70 mm in this study), and $I(t)$ is the intensity of the electric current in Ampere, measured as a function of time with a maximal error of 5%. As the incident pressure is proportional to the square of the current, its amplitude is a positive damped sinusoid.

The targets are glued to the upper electrode using a 50 μm thick adhesive layer that provides a uniform transmission of the load to the target. It has a negligible effect on the load applied on the incident surface of the target since this glue layer is very thin.

Since the impact area is rather large compared to the targets thickness, the influence of edge effects on wave propagation within the samples is negligible. The waves propagate thus normal to the interfaces during a few back and forth within the target and the induced deformation is considered uniaxial at the center of the sample (solicitation mode I).

A schematic side view of the experimental setup is presented on Figure 2. The upper electrode hosts 6 CFRP
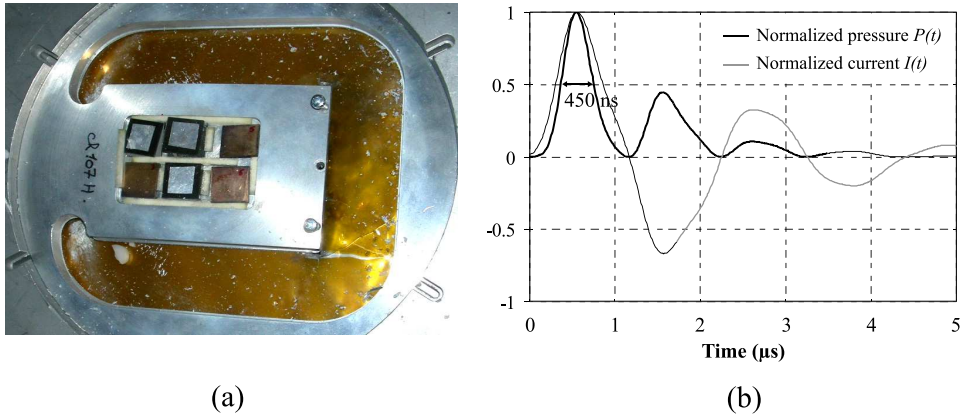
FIG. 1. (a) Electromagnetic cell of the GEPI device (upper cell) and (b) normalized current shape and incident pressure.

(a)   (b)

samples and assemblies and the lower one hosts 6 transparent PMMA samples.

A customized multipoint VISAR (Velocimetry Interferometer System for Any Reflector) (Barker and Hollenbach, 1972) has been used to record the velocity. This interferometer is based on the Doppler shift of the light reflected from the free surface. Its time precision is in the ns range with a 1% resolution between 10 and 10^4 m s^{-1} in our configuration. The sensed spot is of about $50\,\mu$m wide. The free surface velocity is measured at the center of the top side of the CFRP specimens. Reference velocities have been recorded simultaneously at the interface between the lower electrode and the transparent PMMA samples. Due to the symmetry of the strip-line, these measurements provide accurate information on the incident wave arriving on the CFRP specimens. This is useful to correct Eq. (1) for errors resulting from the inaccuracies of the current measurements.

C. Experimental conditions

The conditions of the experiments presented in this study are reported in Table I. The targets are referred A to D for the 8 plies laminates, and E to H for the composite bonded assemblies. The specimens A to D as E to G are similar and have been subjected to an increasing load near their debonding threshold. Targets G and H bonded with two different adhesives, respectively, EA9394 and FM73, have been submitted to a comparable load.

III. NUMERICAL SIMULATION

The experiments have been modeled using the explicit finite elements code ABAQUS$^\copyright$. Structured hexahedral elements
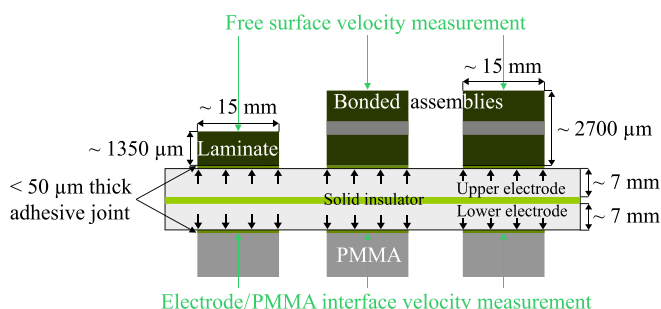

FIG. 2. Experimental set-up of the load region (scale not respected).

have been used to mesh the laminates and the adhesives. The mesh size is estimated by $\Delta L \leq \frac{C_0 \times \tau}{6}$, so the wave propagates through several elements. However, the mesh size has been reduced to $\Delta L = 10\,\mu$m in order to properly represent the interply. No local mesh refinement has been performed. The step time is given by the Courant-Friedrich-Levy relation $\Delta t \leq \frac{\Delta L}{C_0}$, here $\Delta t = 2$ ns and the pulse front does not cross more than one element between two time increments.

A. CFRP laminates and bonded assemblies

The composite laminate is represented by 8 oriented plies between 9 thin epoxy layers. Plies and interplies are stacked together and the interfaces are assumed to be without diffusion on either side. The main hypothesis concerns the geometry, since the layers thickness measured on the cross-sections is considered constant.

The dynamic behaviour of the composite (Thiruppukuzhi and Sun, 2001; Riedel et al., 2004) and of the adhesive is described using an elastic law with the Mie-Grüneisen equation of state, given by relation (2)

$$P - P_{ref} = \frac{\Gamma}{V}(E - E_{ref}), \qquad (2)$$

where P is the pressure, $V = 1/\rho$ is the specific volume (ρ is the density), and E is the internal energy. P_{ref} and E_{ref} are, respectively, the pressure and energy at 0 K. Γ is the Mie-Grüneisen coefficient, which is proportional to the specific volume: $\frac{\Gamma}{V} = \frac{\Gamma_0}{V_0}$.

Properties are given in Table II. The homogenized wave sound velocity within the laminate is calculated at 2880 m s^{-1} on average in the transverse direction.

The delamination is modeled using a cut-off criterion: it occurs once the tensile stress in the trough-thickness direction is higher than the tensile strength.

B. Loading

The load given by relation (1) has been corrected using the velocity recorded at the Aluminum/PMMA interface for each shot. k_p magnitude has been adjusted by varying the incident pressure as an input parameter in the simulation, until the agreement between the experimental and numerical first velocity peak is correct. The electrode mechanical behaviour is described using a Johnson-Cook model

		Geometry		Simulation
Ref	Specimen configuration	Thickness laminate + glue + laminate (μm)	Final state	Incident P_{max} (MPa)
A	8 plies	1360	Intact	335
B	8 plies	1330	Delaminated	387
C	8 plies	1350	Delaminated	521
D	8 plies	1350	Delaminated	759
E	8 plies EA 8 plies	$1245 + 260 + 1215 = 2720$	Intact	455
F	8 plies EA 8 plies	$1215 + 240 + 1210 = 2665$	Debonded	623
G	8 plies EA 8 plies	$1215 + 220 + 1170 = 2605$	Debonded	857
H	8 plies FM 8 plies	$1255 + 525 + 1210 = 2990$	Intact	835

(A $= 2.65$E8 Pa, B $= 4.26$E8 Pa) and the Mie-Grüneisen equation of state, with the properties given in Table II.

Figure 3 shows the experimental and computed velocity at the interface between the lower Aluminum electrode and a PMMA sample. In this example, a 335 MPa load has been used to reproduce the experimental profile.

Experimental and numerical results have the same time evolution for a mesh size of 10 μm with minor amplitude discrepancies on the second emergence. This mesh size and time step provide a good compromise between CPU cost and results precision. The simulation is thus able to reproduce the loading characteristics and its propagation.

IV. LAMINATE BEHAVIOUR UNDER SHORT COMPRESSIVE LOAD

A. Results below the delamination threshold

Figure 4 shows the cross-section of the 8 plies sample A submitted to a 335 MPa load below its delamination threshold. It does not show any observable damage.

The wave propagation within this sample is described on a space-time diagram under uniaxial deformation (Figure 5(a)). The stress history is computed in the whole sample, compression is represented in red and tensile stress in blue. The corresponding computed and experimental free surface velocities are presented in Figure 5(b). The time origin corresponds to the beginning of the load at the incident surface of the sample. The symbols A_1, A_2, and A_3 close to the free surface correspond to the peak numbers reported on the velocity profiles of Figure 5(b), with a slight delay between the beginning of the acceleration at the wave arrival and the local maximum velocity.

The maximal tensile stress is located within the 4th ply at 570 μm from the front surface, where the incident wave reflection crosses the unloading. This value is not far from Antoun's predictive basic model that gives $C_0 \times \tau/2 = 648$ μm with the homogenized sound velocity of 2880 m s^{-1}. The reloads have a limited influence on the tensile stress magnitude but they reduce its duration. The reflections at the interfaces between plies are negligible compared to these principal waves. The wave is contained in the whole thickness of the plate (pulse length $= \tau \times C_0 = 450.10^{-9} \times 2880 = 1.296$ mm) and all the plies have been submitted to a high tensile stress (except the bottom and top plies).

The free surface velocity plotted in Figure 5(b) shows three major peaks, corresponding to the emergence of the load at the back surface. The first acceleration A_1 at 0.47 μs identifies the incident front wave accelerating the free surface, followed by a deceleration due to rarefaction. The velocity peaks A_2 and A_3 correspond to the main wave after propagating three and five times through the whole specimen. These reflections of the main wave are amplified by the simultaneous superposition of the reloads, arriving almost at the same time at the back surface.

The wave velocity is evaluated using the time required for a back and forth within the laminate ($t_{A2-A1} = t_{A3-A2} = 0.94$ μs). It is calculated at: $2 \times$ thickness$_A/t_{A2-A1} = 2 \times 1.36.10^{-3}/0.94.10^{-6} = 2893$ m s^{-1}, which is approximately the homogenized sound velocity of the laminate. This shows that the wave propagates in the elastic regime, well below the Hugoniot elastic limit of the CFRP. This observation is correlated with the fact that no elastic precursor is visible during the first acceleration of the free surface velocity.

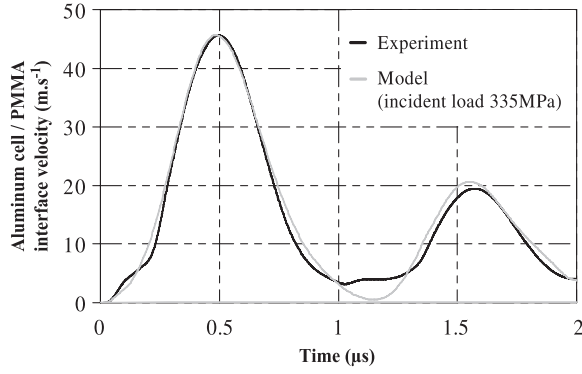|	Initial density (kg m^{-3})	Young's modulus (GPa)	Poisson ratio	Mie Grüneisen coef.	Sound velocity (m s^{-1})	Impedance (g cm^{-2} s^{-1})
Aluminum	2680	70	0.33	2	5336	1.44×10^6
Epoxy	1260	5.2	0.35	0.87	2600	0.33×10^6
Ply dir T	1630	12.6	0.3	2	3000	0.49×10^6
dir L	1630	202	0.27	2	8100	1.32×10^6
EA9394	1360	2.62	0.45	0.8	2600	0.35×10^6
FM73	1200	2.87	0.4	0.8	2200	0.26×10^6

FIG. 3. Comparison between experimental and computed velocity at the Aluminum/PMMA interface (ABAQUS© simulation, mesh size 10 μm, step time 2 ns).

The computations are in relatively good agreement with the experimental measurements for time synchronization. The amplitude discrepancies between simulation and experiment are acceptable during the first 2.5 μs. This result attests that the simulation is relevant to reproduce wave propagation within a composite laminate.

The discrepancies from the emergence A_3 could have been induced by the variation of the proportion of carbon fibres within a ply. Indeed, the local density is different from the homogenized values used in the simulation that assume a uniform fibres distribution. A more accurate ply density could be evaluated from carbon fibres proportion measured on SEM cross-sections and used as an input parameter in the simulation.

Besides, this fluctuation induces local variations of the thickness of the layers (see an illustration of this phenomenon in Figure 4). The layer thicknesses used in the model have been measured in the central zone of the target. However, the sensed spot (50 μm) is still larger than the diameter of the carbon fibres (5 μm) so a mere defect or fibre rupture under the sensed spot would affect the velocity measurement. The improvement of the model requires a better representation of the laminate geometry at the position where the velocity has been recorded.
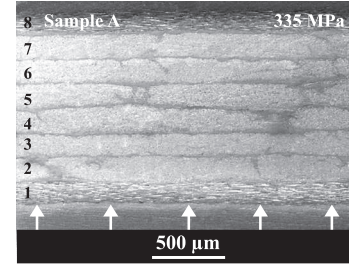

FIG. 4. Microscopic transverse observation of the 8 plies sample A after a load of 335 MPa. The loading zone is indicated by the white arrows.

B. Results above the delamination threshold

Internal tensile stress of sufficient magnitude leads to the delamination of the 8 plies samples B, C, and D. They have been submitted to a load of 387, 521, and 759 MPa, respectively. Figure 6 shows the cross section micrographs of these specimens after the impact. The sample B loaded at 387 MPa shows a small delamination (gap < 25 μm measured on Figure 6(a)) between the 3rd and the 4th ply from the front surface. This damage is not continuous within the laminate and the plies remain stacked. This could be considered as a first stage of damage. It is possible that the adhesion properties of the interply are heterogeneous due to fibre distribution, thickness variations, residual stresses generated during the cooling after the heat treatment. For a higher loading (sample D, Figure 6(c)), discontinuous delamination is spread from the 3rd to the 6th ply because the damage threshold has been reached on a larger thickness. The delamination is interlaminar, showing that the tensile strength of the interply is lower than within the ply.

The wave propagation in the sample B is reported on a space-time diagram (Figure 7(a)), with the corresponding free surface velocity (Figure 7(b)).

An interlaminar delamination is induced between the 3rd and 4th ply at about 1 μs. The dynamic delamination threshold used in this simulation is 296 MPa. The damage location at 790 μm from the free surface is in agreement with the corresponding cross-section (Figure 6(a)). After
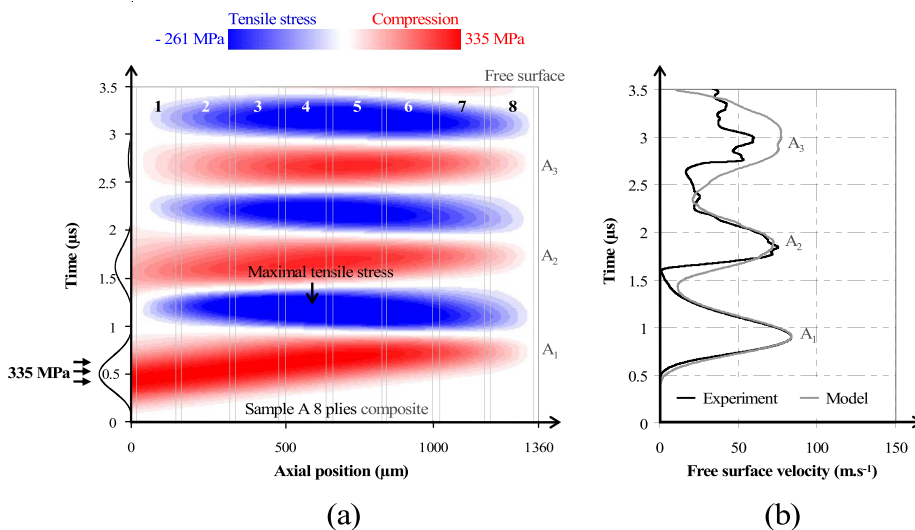

(a)

(b)

FIG. 5. Numerical simulation of the wave propagation within an 8 plies laminate. The incident peak pressure was 335 MPa for sample A without damage. (a) Space-time diagram, compression in red, tensile stress in blue and (b) corresponding experimental and computed free surface velocity (ABAQUS© simulation, mesh size 2 μm, step time 2 ns).
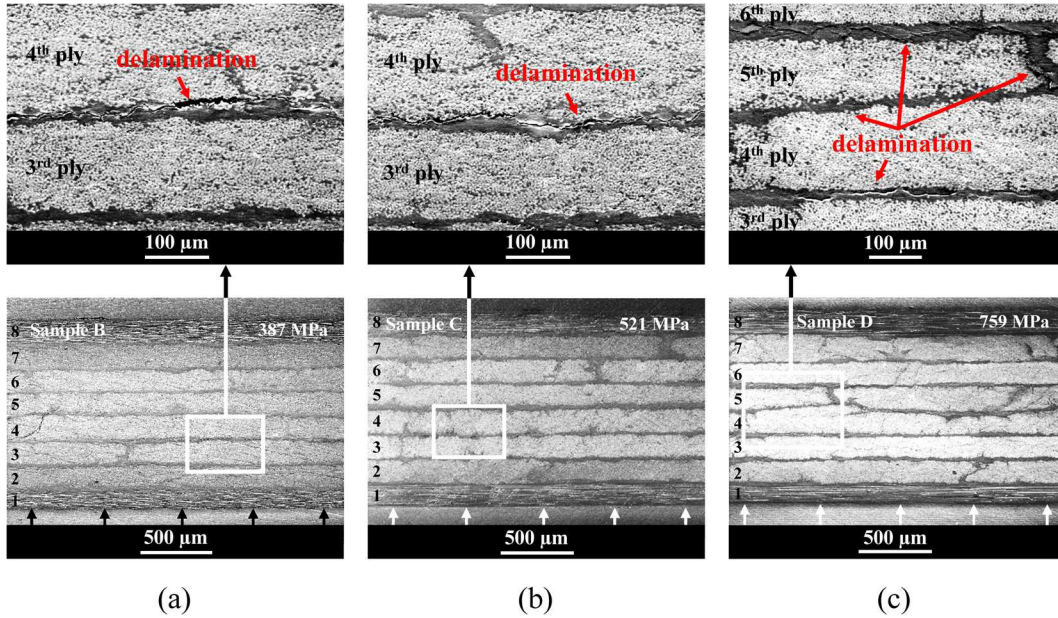
FIG. 6. Microscopic transverse observations with high magnification of the damage of 8 plies laminates. The incident peak pressure was: (a) 387 MPa sample B, (b) 521 MPa sample C, and (c) 759 MPa sample D. The loading zone is indicated by the arrows.

$1\,\mu$s, the residual wave propagates between the free surface and the fracture. The wave emergences B_1 to B_5 occur at higher frequency than in the case without damage. These velocity peaks with a $0.65\,\mu$s period are the signature of delamination.

There are, however, important differences between the experimental and the computed free surface velocity. These discrepancies could be attributed to the basic delamination criterion that does not take into account the local strength variation of the interply when delaminating. Since the delamination is not continuous within the interply layer, it is possible that a portion of the wave has propagated through the heterogeneous damage. As the position of the velocity record cannot be precisely located, it is difficult to represent the local delamination of the target at the location where the velocity has been measured. Besides, the damage behaviour of the epoxy at very high strain rate is not thoroughly established and a progressive damage model might better describe the epoxy behaviour.

Using the inverse approach, the delamination threshold of the composite laminates has been evaluated for an incident pressure of [335–387] MPa. The tensile strength has been then quantified at [255–296] MPa from the computed maximum tensile stress in the interply between the 3rd and the 4th ply. This dynamic tensile limit is much higher than the static one due to the very high strain rate of the solicitation.

The ability of the high amplitude waves to generate tensile stresses of varying intensities within the laminate has been demonstrated. The assessment of the reproducibility of the experiments requires additional tests. Especially stronger loads could completely separate the plies from each other to study the response of an actually delaminated material.
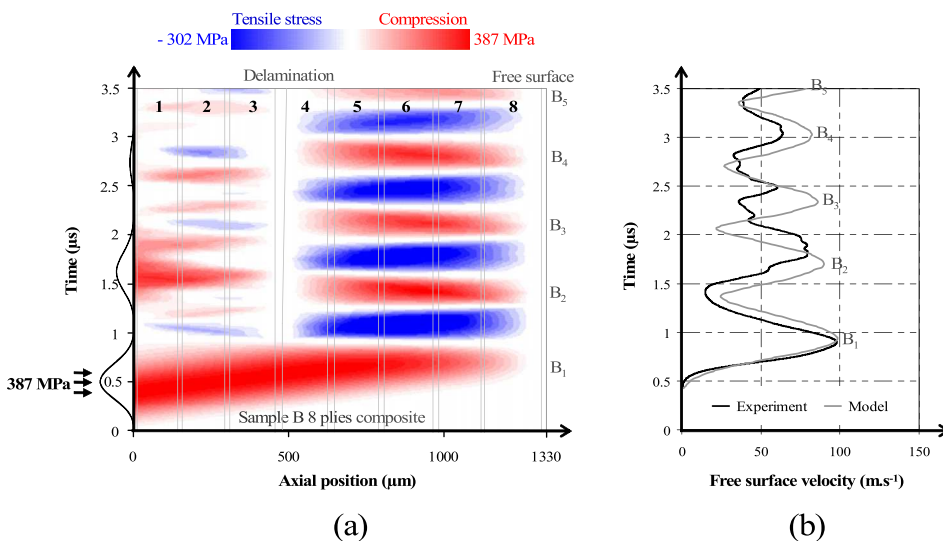

(a)

(b)

FIG. 7. Numerical simulation of the wave propagation within an 8 plies laminate using a cut-off criterion. The incident peak pressure was 387 MPa for sample B. (a) Space-time diagram with induced delamination, and (b) experimental and computed free surface velocity.

Since this first step is validated, the study is extended to its main purpose with composite bonded assemblies to test the adhesion of their interfaces.

V. COMPOSITE BONDED ASSEMBLY BEHAVIOUR UNDER SHORT COMPRESSIVE LOAD

A. Results below the debonding threshold

Figure 8 pictures SEM observation of the bonded assembly E submitted to a 455 MPa load below its debonding threshold. It shows no interface separation or delamination.

The wave propagation within this sample is described on a space-time diagram in Figure 9(a), with the corresponding experimental and computed free surface velocity from 0 to 4 μs in Figure 9(b). They have roughly the same time evolution, even if differences remain for the amplitudes. These discrepancies are again attributed to the simplified representation of the laminates and of the adhesive.

The pulse length still reaches 1300 μm and the tensile stress is spread over the whole sample. The maximal tensile stress is generated when the unloading crosses the incident wave reflection, so the tensile wave is no more superimposed with the compressive one. It is thus located in the 8 plies composite opposite to the impact, and the adhesive is subjected to a lower solicitation. The impedance mismatch at the interface between the laminate and the adhesive is responsible for a slight wave reflection that attenuates the stress within the adhesive. The more important sample thickness emphases the hydrodynamic damping during the wave transit, and this yields to a lower tensile stress. According to the numerical simulations, the tensile stress at the adhesive interface reaches 168 MPa during a few hundreds of ns. This is not sufficient to disbond the assembly.

The laminate has been submitted to a 180 MPa tensile stress without delaminating since this solicitation is below its delamination threshold, previously defined at [255–296] MPa at very high strain rate.

The first acceleration E_1 (Figure 9(b)) from t = 0.9 μs corresponds to the emergence of the incident load. The free surface oscillations have then a period of nearly 0.9 μs between the peaks E_1 to E_4. They notify the arrival of the
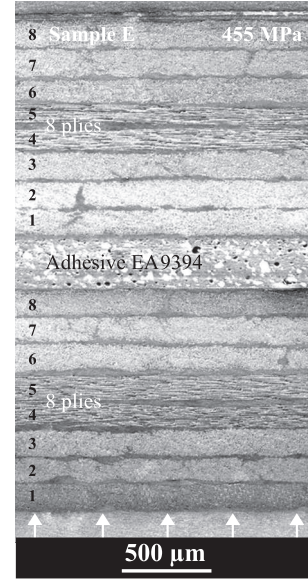

FIG. 8. Microscopic transverse observation of the assembly E bonded with EA9394 after a load of 455 MPa. The loading zone is indicated by the arrows.

reloads at the back surface. A part of the incident wave after a back and forth within the laminate is superimposed to these accelerations. The velocity peak E_3 indicates that the structure has remained intact, since $t_{E3} - t_{E1}$ is equal to twice the transit time of the main wave in the whole assembly: $t_{\text{back and forth}} = 2 \times (\text{thickness}_{\text{laminates}}/C_{0\ \text{laminate}} + \text{thickness}_{\text{adhesive}}/C_{0\ \text{adhesive}}) = 2 \times [(1.245 + 1.215).10^{-3}/2880 + 0.260.10^{-3}/2600] = 1.9\ \mu$s.

B. Results above the debonding threshold

A 623 MPa load has separated the composite laminates of sample F from its adhesive. Figure 10 shows the interface debonding on planar observations (Figure 10(a)) and the cross section of the reconstituted specimen (Figure 10(b)). The failure, mainly in mode I (tensile stress), is adhesive since the disbond has occurred at the interface between the adhesive and the composite. The fractures of the adhesive
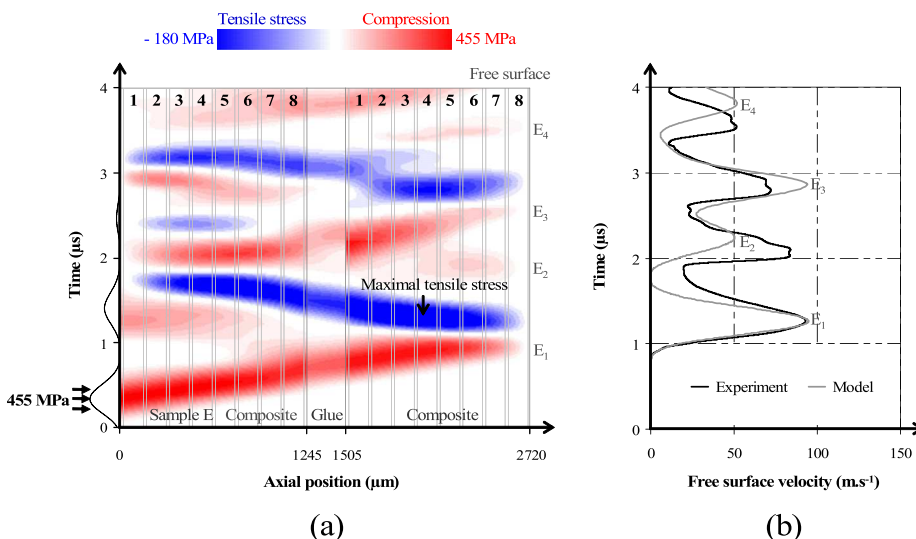

(a)

(b)

FIG. 9. Numerical simulation of the wave propagation within a composite assembly bonded with EA9394. The incident peak pressure was 445 MPa for sample E without debonding. (a) Space-time diagram and (b) experimental and computed free surface velocity (mesh size 2 μm, step time 2 ns).
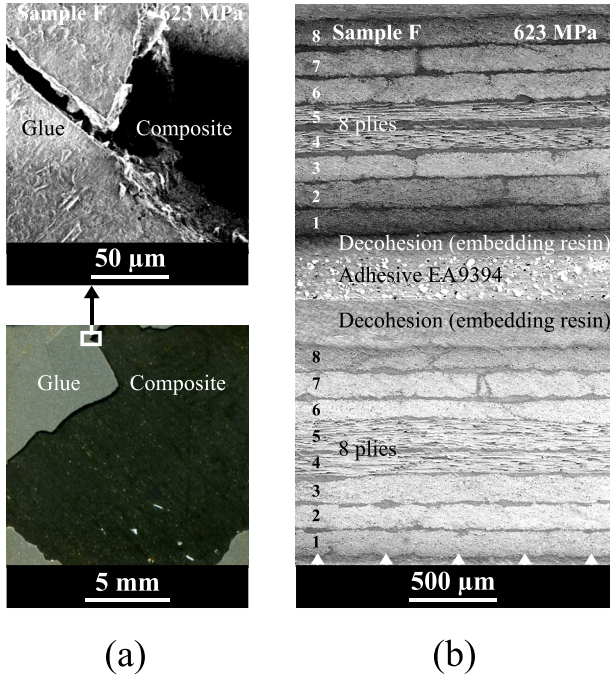
FIG. 10. Microscopic observations of the fracture of the assembly F bonded with EA9394 after a 623 MPa load: (a) planar observations and (b) transverse observation of the reconstituted sample. The loading zone is indicated by the arrows.

layer (cracks normal to the interfaces) could have been induced by the flexural solicitation that has occurred during the removal of the laminate, or by the strength variability along the joint.

Figure 11 shows the space-time diagram and the corresponding experimental and computed free surface velocity for this sample. A cut-off criterion has been used to model the rupture of the interfaces. The velocity profile of sample F has a $0.83 \mu s$ period oscillation from F_1 to F_4 that corresponds to the wave reflection in the debonded laminate. In the experiments, this oscillation is later attenuated and the laminate is ejected at about $75 \, m \, s^{-1}$.

The cut-off model is not properly relevant to describe the evolution of the damage after the rupture of the interface,

since there are important discrepancies between the experimental and numerical free surface velocity (Figure 11(b)). It is possible that the experimental disbond did not completely occur at $1.3 \mu s$ but later, since the secondary tensile stresses are also very high (see Figure 9(a) from $2.6 \mu s$).

The incident pressure threshold of the assemblies bonded with EA9394 is estimated in the interval of [455–623] MPa. The numerical simulations show that the tensile strength of the interfaces is included in [168–230] MPa at very high strain rate. It is below the threshold of the laminate, previously evaluated at [255–296] MPa. This shows that the bond interface is weaker than the laminate. The threshold interval could be refined by performing further experiments between [455 and 623] MPa.

VI. SENSITIVITY OF THE BOND STRENGTH

The ability of the technique to differentiate the level of strength is demonstrated in this section. Composite assemblies bonded with EA9394 and FM73 have been subjected to a similar load. The Figure 12 shows the experimental free surface velocities recorded during these tests.

The failure or survival of the assembly is established using the motion of the free surface. The first velocity peaks referred G_1 and H_1 show a small difference of amplitude: 179 and $162 \, m \, s^{-1}$ for targets G and H due to their difference of thickness. These samples have been subjected to a similar load, evaluated at, respectively, 857 and 835 MPa using numerical simulation (see Sec. III B).

Their velocity profiles are later different. The 3rd velocity peak H_3, recorded $1.8 \mu s$ after the occurrence of the first wave H_1, means that the wave has propagated three times through the assembly H. This indicates that the sample H remains intact (see the wave propagation on Figure 9). On the other side, the free surface of sample G shows an oscillation with a 750 ns period, equal to twice the transit time of the wave in the debonded laminate.

Figure 13 shows the cross-section micrographs of the specimens G and H. This confirms that the sample H bonded with FM73 remains intact after the solicitation. The sample G bonded with EA9394 is debonded at the two interfaces
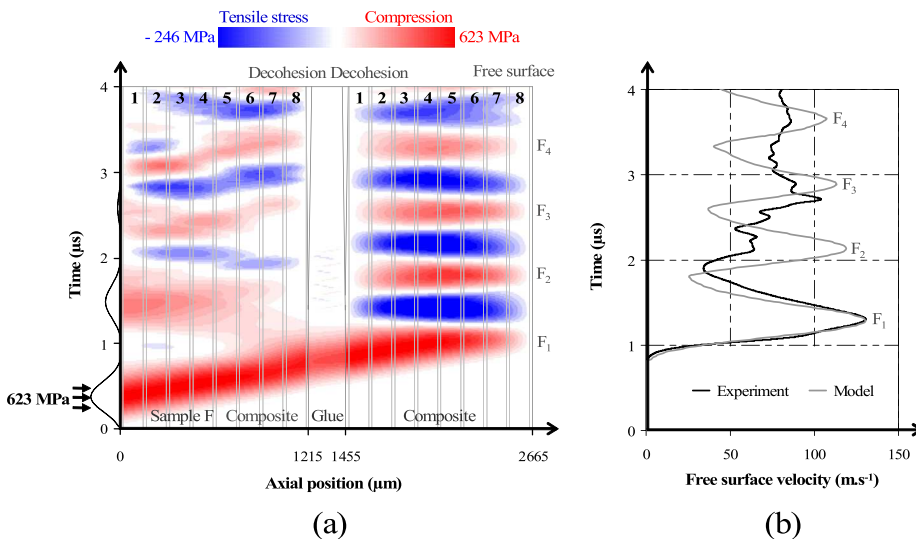

(a)

(b)

FIG. 11. Numerical simulation of the wave propagation within a composite assembly bonded with EA9394 using a cut-off criterion. The incident peak pressure was 623 MPa for sample F. (a) Space-time diagram with induced debonding and (b) experimental and computed free surface velocity.
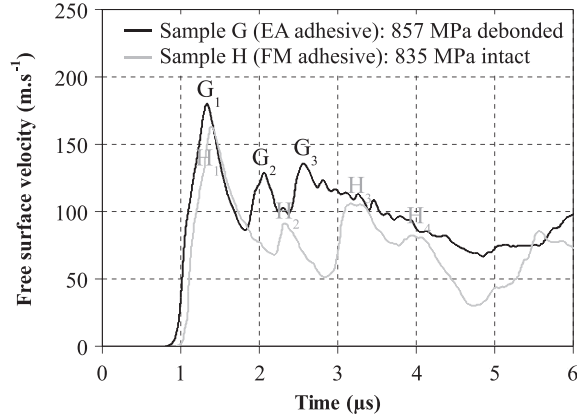
FIG. 12. Free surface velocity recorded on the assemblies bonded with EA9394 and FM73 submitted to a load of 0.85 GPa.
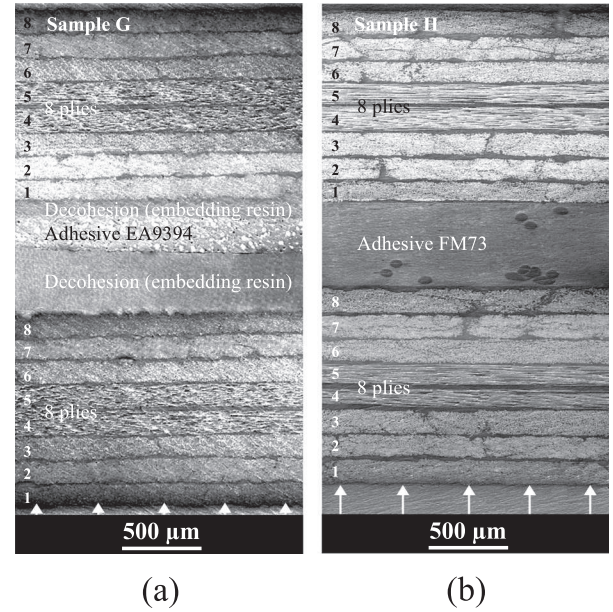

(a)   (b)

FIG. 13. Microscopic transverse observations of composite assemblies after a load of 0.85 GPa. The samples have been bonded using: (a) EA9394, reconstituted sample G, and (b) FM73, sample H. The loading zone is indicated by the arrows.

between the laminates and the adhesive. The technique is thus sensitive to the bond strength. These results are in agreement with the peel-tests performed on similar samples (Sec. II A).

The Table III summarizes the results for the 3 specimen configurations, with an estimation of their tensile strength. A simulation of the response of the assembly H bonded with FM73 has been carried out. It indicates that the interfaces of this assembly have been submitted to a tensile stress of 300 MPa during a few hundreds of ns without debonding. This means that the bond is optimal since it is as strong as the laminate (Gilath *et al.*, 1992).

The composite laminate near the free surface of this sample is still intact after a 314 MPa tensile stress between its 3rd and 4th ply. This solicitation is a bit higher than the composite dynamic tensile strength previously determined. This could be attributed to the variation of strength within the laminate. It is also possible that the cure process required for the FM73 adhesive has slightly modified the laminate properties by promoting the interlaminar and interply diffusion.

VII. CONCLUSION

Adhesion testing using short compressive load has many advantages compared to the conventional inspection methods. The adhesive strength is estimated normal to the interface, with a quasi uniaxial deformation (mode I). It remains non-destructive since a calibrated load only damages weak samples. In the future, the GEPI device has to be replaced by a high power laser. It has the ability to test structures of any shape without mechanical contact, and the technique would be actually non-destructive.

However, this approach has several limitations such as the cost of the loading source, and the need to access to the free surface. Ultrasonic tools could be used to detect the disbond after the proof-test (Monchalin, 1986; Perton *et al.*, 2010), but kissing bonds will not be detected this way. A restriction on the sample thickness also remains due to wave diffraction, but some experiments have been successfully performed on specimens up to 25 mm thick (Bossi *et al.*, 2009).

The response of composite assemblies to a dynamic load induced by the GEPI device has been developed in this paper. Experiment and simulation have shown that intense brief loads are able to generate a tensile stress and disbond the specimens. The load with a 450 ns pulse duration is appropriate to test the 3 mm thick assemblies even if the maximal tensile stress is not directly generated at the interface to verify. The results clearly evidence the ability of the technique to estimate the strength between the plies of a laminate ([255–296] MPa at very high strain rate) or between a laminate and its adhesive, and to differentiate the bond quality. This dynamic strength of the bond interfaces has been estimated between 168 and 230 MPa and higher than 300 MPa, respectively, for the EA9394 and FM73 adhesive.

A full knowledge of the behaviour of the adhesive material under shock and a better representation of the local geometry of the samples are still required to achieve a tight fit

TABLE III. Debonding threshold of the specimens.

Specimen configuration—Total thickness (μm)	Incident pressure threshold (MPa)	Tensile strength at very high strain rate (MPa)	Localization of the damage
8 plies composite—1350	[335–387]	[255–296]	(interply 3–4th ply)
8 plies EA 8 plies—2680	[455–623]	[168–230]	(adhesive/composite interface)
8 plies FM 8 plies—2990	>835	>300	none

between simulation and experiment. The models should also include a damage criterion that takes into account the progressive delamination and includes a heterogeneous distribution of the strength limit within the interply.

Further works concern the application of the technique to weak bonds in order to validate the sensitivity of the test. The use of high power laser with variable pulse duration would give the ability to test thicker assemblies.

ACKNOWLEDGMENTS

Abrate, S., *Impact on Composite Structures* (Cambridge University Press, 1998).

Adams, R. D., and Cawley, P., NDT Int. **21**, 208–222 (1988).

Adams, R. D., and Drinkwater, B. W., NDT & E International **30**, 93 (1997).

Antoun, T., Seaman, L., Curan, D. R., Kanel, G. I., Razorenov, S. V., and Utkin, A. V., *Spall Fracture* (Springer, New York, 2003), pp. 176–197.

Arrigoni, M., Cuq-Lelandais, J. P., Boustie, M., Gay, E., and Berthe, L., *An industrial challenge based on the wave propagation : the shock adhesion test*, 2012 in *Wave Propagation* (Academy Publish Ed, WY, USA).

Barker, L. M., and Hollenbach, R. E., J. Appl. Phys. **43**, 4669–4675 (1972).

Barnes, N., Bourne, N. K., and Millet, J. C. F., in Proceedings of APS Shock Compression of Condensed Matters (Atlanta, 2001), pp. 135–138.

Bolis, C., Berthe, L., Boustie, M., Arrigoni, M., Barradas, S., and Jeandin, M., J. Phys. D: Appl. Phys. **40**, 3155–3163 (2007).

Bossi, R. H., Housen, K. R., and Shepherd, W. B., Application of Stress Waves to Bond Inspection, SAMPE 2004 Proceeding, Long Beach, CA., May 16–20, 2004.

Bossi, R. H., Housen, K. R., and Walters, C., Laser Bond Inspection Device for Composites: Has the Holy Grail Been Found?, Nondestructive Testing Information Analysis Center, Vol. 30, No. 2, 2005.

Cytec FM73, Cytec Materials Database, Technical Service (Havre de Grace, USA, 2009).

Datta, S. K., *Comprehensive Composite Materials*, edited by T. W. Chou (Elsevier, Oxford, 2000), Vol. 1, Chap. VIII, pp. 511–558.

De Rességuier, T., Berterretche, P., and Hallouin, M., Int. J. Impact Eng. **31**, 545–557 (2005).

Frescaline, L., and Avrillaud, G., U.S. patent 6,838,786 (2005).

Gay, E., Ph.D. dissertation, Arts et Métiers ParisTech, France, 2011.

Gay, E., Berthe, L., Boustie, M., Arrigoni, M., Mercier, P., and Bénier, J., Matér. Techn. **100**, 703–712 (2012).

Gilath, I., Eliezer, S., and Shkolnik, S., J. Compos. Mater. **24**, 1138–1151 (1990).

Gilath, I., Englman, R., Jaeger, Z., Buchman, A., Segal, E., and Dodiuk, H., I.A. Report 2148, 1992.

Gupta, V., Argon, A. S., Cornie, J. A., and Parks, D. M., Mater. Sci. Eng. A **126**, 105–117 (1990).

Gupta, V., Pronin, A., and Anand, K., J. Compos. Mater. **30**, 722–747 (1996).

Guyott, C. C. H., and Cawley, P., NDT Int. **21**, 233–240 (1988).

Hereil, P. L., and Avrillaud, G., J. Phys. IV France **134**, 535–540 (2006).

ITHPP, France patent°99.08771, U.S. patent 10/019,943 (1999).

Loctite Aerospace, Technical Service Laboratory Report: Thick Adherent (KGR-1) Testing for Structil EA9394, Structil SNPE (2002).

Millett, J. C. F., Bourne, N. K., Meziere, Y. J. E., Vignjevic, R., and Lukyanov, A., Compos. Sci. Technol. **67**, 3253–3260 (2007).

Monchalin, J. P., IEEE Ultrason., Ferroelectr., Freq. Control **33**, 485–499 (1986).

Parga-Landa, B., Vlegels, S., Hernández-Olivares, F., and Clark, S. D., Compos. Struct. **45**(2), 125 (1999).

Pethrick, R. A., Compr. Compos. Mater. **5**, 359-392 (2000).

Perton, M., Blouin, A., and Monchalin, J. P., J. Phys. D: Appl. Phys. **44**, 034012 (2010).

Riedel, W., Nahme, H., and Thoma, K., Proceedings of Shock Compression of Condensed Matter (Melville, 2004), pp. 701–714.

Rokhlin, S. I., and Marom, D., J. Acoust. Soc. Am. **80**, 585–590 (1986).

Thiruppukuzhi, S. V., and Sun, C. T., Compos. Sci. Technol. **61**, 1–12 (2001).

Vossen, J. L., *in Adhesion Measurement of Thin Films. Thick Films, and Bulk Coatings*, edited by K. L. Mittal (ASTM, Philadelphia, 1978), Vol. 640, pp. 122–133.

Yu, A., and Gupta, V., Compos. Sci. Technol. **58**, 1827–1837 (1998).